One-Dimensional Surface Plasmon Photonic Crystal Slab (SPPCS) for a Nanophotodiode

Kyungjun Song and Pinaki Mazumder, *Fellow, IEEE*

***Abstract*—For miniaturization of a photodiode, we present a new design concept to increase photogeneration rate in a small active domain by using subwavelength structures consisting of surface plasmon photonic crystal slab (SPPCS) acting like a near-field generator and an antireflection coating. The polarizability of rectangular metallic cylinder predicts surface plasmon (SP) resonance frequency in the SPPCS photodiode. Thus, the enhanced near-field intensity arising from SP resonant oscillation has a potential to solve the low photogeneration problem. In addition, photonic band structure dramatically changes TM photonic maps with extraordinary transmission and low reflection, thereby leading to an efficient nanophotodiode.**

***Index Terms*—Absorption, nanophotodiode, polarizability, reflection, surface plasmon photonic crystal slab (SPPCS), TM photonic maps, transmission.**

I. Introduction

THE periodic surface plasmon photonic crystal slab (SPPCS) modifies photonic properties of a metallic film by artificially tailoring a metallic subwavelength topology, thus leading to dramatic change of surface plasmon (SP) dispersion curves. Especially, the strong near-field confinement and enhanced electromagnetic (EM) transmission of SPPCS generates considerable interest because this engineered SP dynamics opens up new possibilities and promising optoelectronic technology [1]–[6]. For example, the ability to transmit EM field through the SPPCS could increase the efficiency of photonic devices, such as TM polarizer [7] and optical filter [8]. In addition, the capability to increase SP near-field intensity has large potential in optoelectronic devices, such as photovoltaics [9] and LED [10].

In this paper, we focus on a new way to enhance the photogeneration rate for a nanophotodiode by using 1-D SPPCS. In general, the conventional photodiode usually use an antireflection layer [see Fig. 1(a)] to decrease reflection loss in the semiconductor material, thereby obtaining maximum far-field intensity. However, this small reflection loss method has some limitations for a miniaturization of the optical circuitry. First of all, the size of antireflection coating is almost comparable to the wavelength of light. Furthermore, for the nanophotodiode, it is necessary to have a thinner depletion layer and small active semiconductor [11], thus resulting in the small amount of photogeneration rate because of smaller active semiconductor region under the far-field optical field density. To overcome dimension issue of antireflection coating and low photogeneration rate in the small semiconductor layer of the nanophotodiode, the SPPCS [see Fig. 1(b)] could be the best solution for following three reasons: 1) the SPPCS building blocks have the nanoscale dimensions; 2) the localized and delocalized SP modes from SPPCS concentrates strong photons to a small semiconductor layer; 3) TM polarized wave efficiently transmits through SPPCS, thus behaving like an antireflection coating.

Manuscript received November 11, 2008; revised May 22, 2009; accepted August 24, 2009. Date of publication September 29, 2009; date of current version July 9, 2010. This work was supported in part by an Air Force Office of Scientific Research under Grant FA9950-06-1-0493. The review of this paper was arranged by Associate Editor H. Misawa.

K. Song is with the Department of Mechanical Engineering, University of Michigan, Ann Arbor, MI 48109-2121 USA (e-mail: songk@umich.edu).

P. Mazumder is with the Department of Electrical Engineering and Computer Science, University of Michigan, Ann Arbor, MI 48109-2121 USA (e-mail: mazum@eecs.umich.edu).

Color versions of one or more of the figures in this paper are available online at http://ieeexplore.ieee.org.

Digital Object Identifier 10.1109/TNANO.2009.2033057

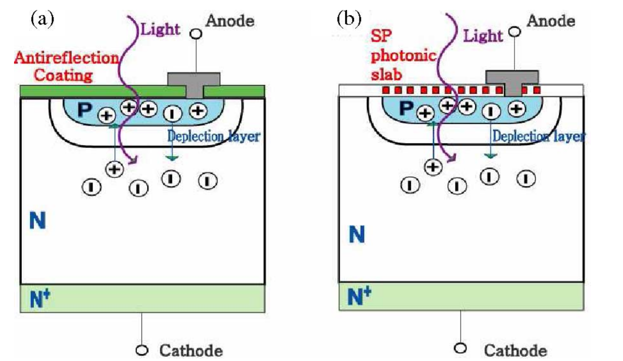

Fig. 1. (a) Conventional photodiode with an antireflection coating. (b) SPPCS for a photodiode.

II. Dimensionless Reduced Polarizablity of Rectangular Cylinder

Fig. 2(a) and (b) show schematics of our SPPCS photodiode of consisting of Si active semiconductor and Au (gold) photonic slab. The grating structure is composed of two different media with Au and air ($n = 1$). The frequency dependent optical properties of Au [12] and Si [13] are obtained by interpolating the Johnson's and Palik's experimental data as displayed in Fig. 2(c). First, we have calculated the polarizability of the rectangular metallic cylinder [see Fig. 2(d)] to obtain SP resonant frequency for an efficient near-field EM confinement in the semiconductor layer. Physically, when the wavelength of the incident field is large compared to the geometry of the metallic rectangular cylinder, the confined electron cloud generates the dipole-like polarization, thus explaining the SP resonance in the 2-D rectangular geometry. This polarizability of the rectangular metallic cylinder placed at free space ($n = 1$) is given by [14]

$$p_L = -8\chi ab(C_1 - C_2(a^2 - b^2)) \quad (1)$$

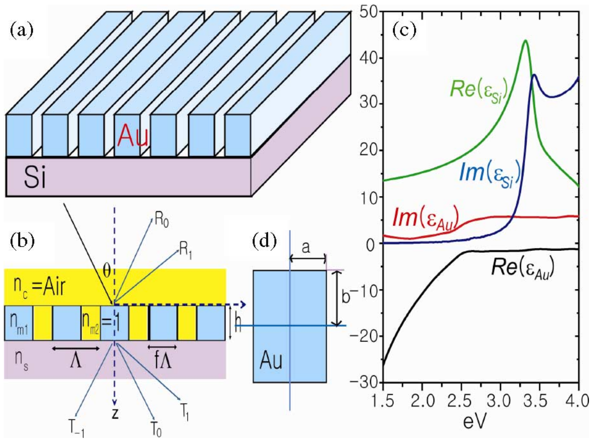

Fig. 2. (a) Schematic view of SPPCS. (b) Geometry of SPPCS. The parameters are defined as in the figure: Λ is the periodicity, $f\Lambda$ is width of Au, and h is the thickness of the SPPCS. (c) Complex dielectric constant of Au and Si was obtained by experimental data based on the cubic regression method. (d) Cross section of Au rectangular cylinder.

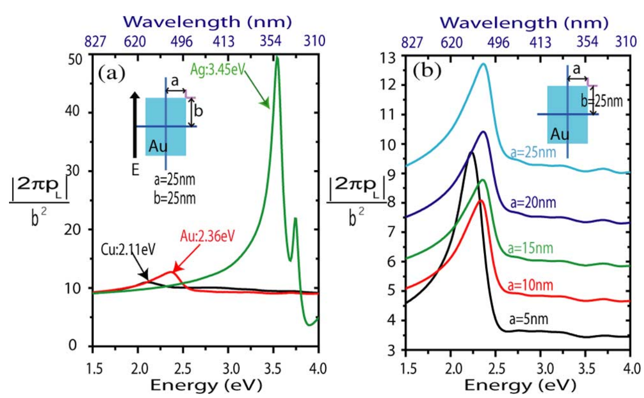

Fig. 3. (a) Dimensionless reduced polarizability of rectangular SP cylinder as a function of photon energy. These curves are obtained from the cubic spline method by using the Johnson's experimental optical data of three different noble metals: Cu, Au, and Ag. (b) Dimensionless reduced polarizability of Au rectangular cylinder with different geometry ratio (a/b).

where χ is the electric susceptibility given by $\chi = (\varepsilon_m - 1)/(4\pi)$, $\varepsilon_m(\omega) = \varepsilon_r(\omega) + j\varepsilon_i(\omega)$ is the complex dielectric function of metal, $C_1(\varepsilon_m, a, b)$, and $C_2(\varepsilon_m, a, b)$ are function of ε_m, a, and b. Eyges and Gianino have derived a detailed mathematical formulation for the polarizability of rectangular dielectric cylinders by using the Green function analysis [14]. Fig. 3(a) shows the magnitude of dimensionless reduced polarizability $2\pi|p_L|/b^2$ for rectangular SP cylinder ($a = 25$ nm and $b = 25$ nm) by using the Johnson's experimental data of three different noble metals: Cu (copper), Au (gold), and Ag (silver) [12]. As can be seen, compared with Cu and Au, Ag shows the maximum polarizability, thus generating strong EM field enhancement. However, the imaginary permittivity of Si tremendously increases from 3.0 eV as shown in Fig. 2(c), thus the resonance frequency (3.49 eV) of Ag rectangular cylinder lies in the strong damping region. Therefore, we choose Au to minimize far-field damping loss in the semiconductor medium at the resonant condition (2.36 eV) and obtain the efficient delocalized SP modes at the lower frequency. In Fig. 3(b), the magnitude of polarizability of Au cylinder can be manipulated by changing a (width) and b (height). As the ratio ($r = a/b$, b is 25 nm) decreases, the magnitude of polarizability of Au also decreases because of the capacity of electron cloud inside the metallic cylinder.

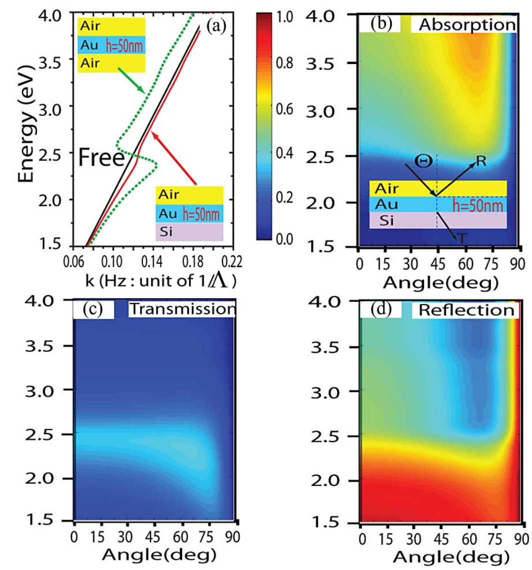

Fig. 4. TM photonic maps for a metallic slab (air/Au/Si) with thickness 50 nm. These figures are presented for frequency from 1.5 to 4 eV and incident angles from 0° to 90°. (a) Dispersion relations $\omega(k)$ for SP on the thin films: air/Au/air (green line) and air/Au/Si (red line). (b) Absorption map of thin film (air/Au/Si). (c) Transmission map of thin film (air/Au/Si). (d) Reflection map of thin film (air/Au/Si).

III. Photonic Map of SPPCS

In order to check SP resonant modes have an effect on the efficiency of SPPCS photodiode, we have employed the rigorous coupled-wave analysis (RCWA) to obtain TM photonic maps including absorption, transmission, and reflection [15]. To demonstrate the usefulness of SPPCS for the photodiode, we first investigate the Au film (no grating structure) with thin thickness ($h = 50$ nm) shown in the inset of Fig. 4(a). First, we investigate the dispersion relations $\omega(k)$ for SP on the thin films by considering EM boundary conditions at the two interfaces. The main reason is that the simplest way to understand the photonic behavior is to examine the SP dispersion relations. As can be seen, even (symmetric) SP modes and free space in a symmetric environment air/Au/air intersect with the critical point (2.48 eV). Fundamentally, SP modes in the symmetric gap environment can be classified as even (symmetric) modes and odd (antisymmetric) modes with respect to mirror symmetry. In this paper, we ignore the antisymmetric SP modes because symmetric SP modes are fundamental modes, for which SP modes have the smallest nodes. Similarly, the SP modes and free space in the antisymmetric environment air/Au/Si almost intersect the critical point. Physically, this means that when the frequency is below the critical point, the strong momentum mismatch occurs between incident wave and SP modes, thus producing the high reflection spectrum. However, above the critical point, the small momentum mismatch leads to the strong absorption inside the

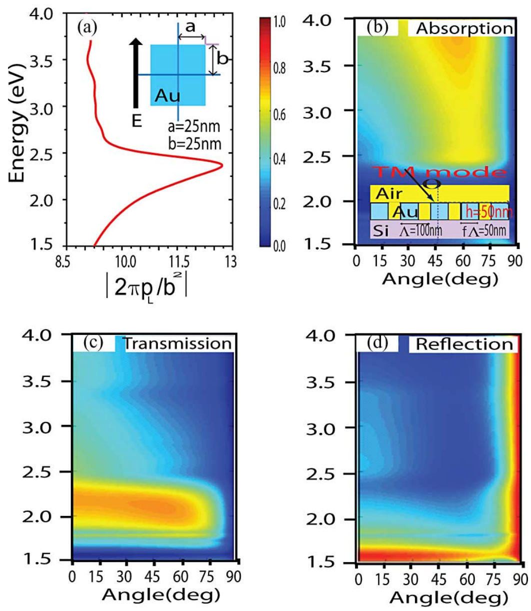

Fig. 5. TM photonic maps for a SPPCS (air/Au/Si) with periodicity (Λ = 100 nm), width ($f\Lambda$ = 50 nm), and thickness (h = 50 nm). These figures are presented for frequency from 1.5 to 4 eV and incident angles from 0° to 90°. (a) Dimensionless reduced polarizability of Au rectangular SP cylinder as a function of photon energy. (b) Absorption map of SPPCS. (c) Transmission map of SPPCS. (d) Reflection map of SPPCS.

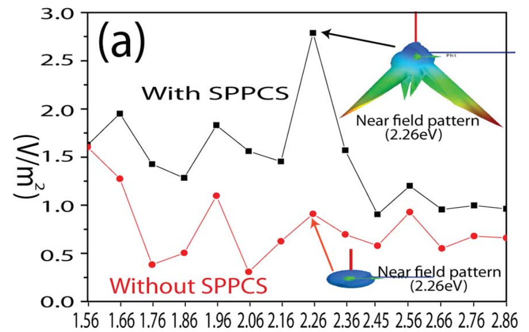

Fig. 6. Comparison magnitude of near-field density between SPPCS photodiode and uncoated SPPCS photodiode.

metallic film. More specifically, Fig. 4(b)–(d) give us a clue on how the critical frequency (2.48 eV) has influenced on the optical behavior of thin film. In Fig. 4(b)–(d), the absorption, transmission, and reflection maps of air/Au/Si ranging from 1.5 to 4 eV (photonic energies) and 0° to 90° (incident angles) are displayed. Below the critical frequency (2.48 eV), most EM waves reflected because of strong momentum mismatch. However, at the critical frequency, the peak of transmission occurs as predicted by the SP dispersion analysis. As the frequency increase above the critical point, most incident EM waves absorb in the Au film.

These thin film photonic maps can be significantly modified by creating the photonic band structure. Fig. 5 demonstrates the photonic maps of SPPCS with periodicity ($\Lambda = 100$ nm), width ($f\Lambda = 50$ nm), and thickness ($h = 50$ nm). As can be seen in Fig. 5(a), the maximum reduced polarizability of rectangular SP cylinder occurs at the resonant frequency (2.36 eV), thus leading to strong SP generator, thereby increasing the EM field intensity and enhancing the photogeneration rate in the Si medium. As shown in Fig. 5(b), even though absorption map of SPPCS does not significantly changed by creating the photonic band structure, strong SP resonance coupling between metallic rectangular cylinders leads to the extraordinary transmission and low reflection in angle-frequency domain as shown in Fig. 5(c) and (d).

IV. FEM Simulation of a Nanophotodiode

It has been shown that the photonic maps of SPPCS can be tailored, thus obtaining efficient light transmission in the active medium, we now focus on the realistic simulation for demonstrating strong light confinement and enhanced transmission in the SPPCS photodiode. In Fig. 6, we show that magnitude of near-field density (black line) of SPPCS photodiode under the incident TM plane wave with incident angle $\theta = 0$ (degree) and amplitude $E = 1$ V/m (field density = 0.707 V/m^2) for following SPPCS geometry: periodicity ($\Lambda = 100$ nm), width ($f\Lambda = 50$ nm), and thickness ($h = 50$ nm). Furthermore, contrast to previous RCWA structure, we make small air gap (5 nm) between SPPCS and Si active medium to efficiently distribute strong near-field at the surface of semiconductor layer. These graphs have been calculated by the near-field pattern obtained by using high frequency structure simulator (HFSS) simulation based on the finite-element method (FEM). As predicted by polarizability analysis, the magnitude plot of near-field density is similar to the magnitude graph of polarizability of rectangular SP cylinder, thus justifying the validity of polarizability method as shown in Fig. 5(a).

As shown in Fig. 6, the near-field pattern has strong field profile at the corner of metallic rectangular cylinder. Furthermore, strong near-field density profile between 2.16 and 2.36 eV can be explained by the electron cloud oscillation in the confined metallic cylinder. Even though the zigzag shape can be affected by numerical noises from HFSS, the obvious magnitude difference between SPPCS photodiode and uncoated SPPCS photodiode verify the usefulness of SPPCS for the near-field enhancement. More specifically, the SPPCS generates to strong near-field intensity (2.8 V/m^2) at the resonant frequency 2.26 eV, this value is four orders of magnitude more compared to incident far-field intensity (0.707 V/m^2). The small difference (0.01 eV) of resonant frequency between polarizability calculation and FEM simulation method may be due to the fact that SP coupling between rectangular structures changes the location of resonant modes of SPPCS. In addition, the SPPCS photodiode gives a high value of directivity compared to uncoated SPPCS structure, thus focusing on strong near-field in the active semiconductor layer. Fig. 7(a)–(c) show the snapshots of magnitude of scattered E-field for three different frequencies. Especially, as shown in Fig. 7(a), at the low frequency (1.66 eV), the strong E-field greater than $E = 2$ V/m occupies most active layer because the large wavelength generates delocalized SP modes and localized SP modes, and the optical properties of Si efficiently lead to confine the strong field intensity in the active medium.

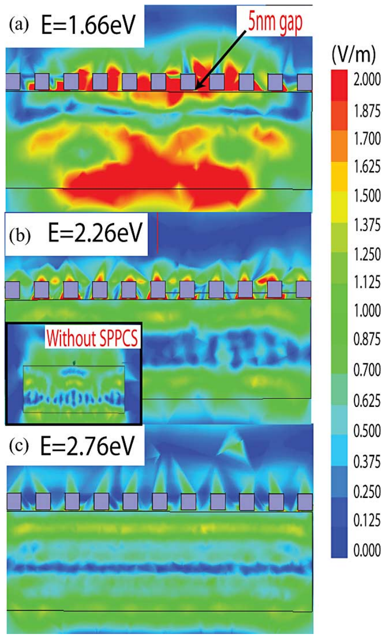

Fig. 7. (a) Snapshot of magnitude of scattered *E*-field at 1.66 eV. (b) Snapshot of magnitude of scattered *E*-field at 2.26 eV. (c) The snapshot of magnitude of scattered *E*-field at 2.76 eV.

Fig. 7(b), at the resonant frequency (2.26 eV), shows that localized SP modes from rectangular structures generate the strong near-field intensity and extraordinary transmission compared to uncoated SPPCS photodiode as shown in the inset of Fig. 7(b). As the frequency increases up to 2.76 eV, the SPPCS structure almost acts like an antireflection coating structure as given in Fig. 7(c).

V. Conclusion

In summary, we have presented a new SP nanophotodiode architecture based on 1-D SPPCS. Specifically, at the resonant frequency (2.26 eV), the four-order increase of near-field intensity (FEM calculation) and almost 70% EM transmission (RCWA calculation) has been demonstrated. The building geometry and noble metals of SPPCS can be changed for the purpose of optimizing EM transmission, near-field generator, and broadband sensitivity. Undoubtedly, this concept is extensible to the various promising photodetector applications, such as solar cell technology and molecular bio sensing.

References

[1] A. Christ, S. G. Tikhodeev, N. A. Gippius, J. Kuhl, and H. Giessen, "Waveguide-plasmon polaritons: Strong coupling of photonic and electronic resonances in a metallic photonic crystal slab," *Phys. Rev. Lett.*, vol. 91, pp. 183901-1–183901-4, 2003.

[2] F. J. Garcia-Vidal and L. Martin-Moreno, "Transmission and focusing of light in one-dimensional periodically nanostructured metals," *Phys. Rev. B*, vol. 66, pp. 155412-1–155412-10, 2002.

[3] C. Genet and T. W. Ebbesen, "Light in tiny holes," *Nature*, vol. 445, pp. 39–46, 2007.

[4] F. J. G. de Abajo, "Colloquium: Light scattering by particle and hole arrays," *Rev. Mod. Phys.*, vol. 79, pp. 1267–1290, 2007.

[5] N. Garcia and M. Nieto-Vesperinas, "Theory of electromagnetic wave transmission through metallic gratings of subwavelength slits," *J. Opt. A: Pure Appl. Opt.*, vol. 9, pp. 490–495, 2007.

[6] E. Moreno, F. J. Garcia-Vidal, D. Erni, J. I. Cirac, and L. Martin-Moreno, "Theory of plasmon-assisted transmission of entangled photons," *Phys. Rev. Lett.*, vol. 92, pp. 236801-1–236801-4, 2004.

[7] Z. Y. Yang and Y. F. Lu, "Broadband nanowire-grid polarizers in ultraviolet-visible near-infrared regions," *Opt. Exp.*, vol. 15, pp. 9510–9519, 2007.

[8] W. L. Barnes, A. Dereux, and T. W. Ebbesen, "Surface plasmon subwavelength optics," *Nature*, vol. 424, pp. 824–830, 2003.

[9] N. C. Panoiu and R. M. Osgood, "Enhanced optical absorption for photovoltaics via excitation of waveguide and plasmon-polariton modes," *Opt. Lett.*, vol. 32, pp. 2825–2827, 2007.

[10] J. Vuckovic, M. Loncar, and A. Scherer, "Surface plasmon enhanced light-emitting diode," *IEEE J. Quantum Electron.*, vol. 36, no. 10, pp. 1131–1144, Oct. 2000.

[11] T. Ishi, J. Fujikata, K. Makita, T. Baba, and K. Ohashi, "Si nano-photodiode with a surface plasmon antenna," *Jpn. J. Appl. Phys. Part 2: Lett. Exp. Lett.*, vol. 44, pp. L364–L366, 2005.

[12] P. B. Johnson and R. W. Christy, "Optical-constants of noble-metals," *Phys. Rev. B*, vol. 6, pp. 4370–4379, 1972.

[13] E. D. Palik and G. Ghosh, *Handbook of Optical Constants of Solids*. Orlando, FL: Academic, 1985.

[14] L. Eyges and P. Gianino, "Polarizabilities of rectangular dielectric cylinders and of a cube," *IEEE Trans. Antennas Propag.*, vol. AP-27, no. 4, pp. 557–560, Jul. 1979.

[15] M. G. Moharam, E. B. Grann, D. A. Pommet, and T. K. Gaylord, "Formulation for stable and efficient implementation of the rigorous coupled-wave analysis of binary gratings," *J. Opt. Soc. Amer. A: Opt. Image Sci. Vis.*, vol. 12, pp. 1068–1076, 1995.

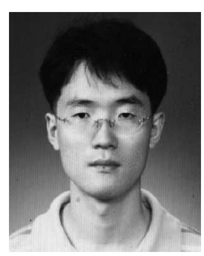

Kyungjun Song received the B.S. degree in mechanical engineering from Seoul National University, Seoul, Korea, and the M.S. degree in mechanical engineering from the University of Michigan, Ann Arbor, in 2002 and 2004, respectively. He is currently working toward the Ph.D. degree in mechanical engineering from the University of Michigan.

He is a Graduate Student Research Assistant in the Electrical Engineering and Computer Science Department, University of Michigan. His current research interests include the modeling, simulation, and design of plasmonic nanoarchitecture.

Pinaki Mazumder (F'99) received the Ph.D. degree from the University of Illinois at Urbana-Champaign, Urbana-Champaign, in 1988.

He is currently a Professor in the Department of Electrical Engineering and Computer Science, University of Michigan (UM), Ann Arbor. He is on leave for 1 year from the UM to serve as the lead Program Director of the Emerging Models and Technologies Program at the U.S. National Science Foundation, Arlington, VA. For six years, he was with industrial Research and Development centers that included AT&T Bell Laboratories, Murray Hill, NJ, where in 1985, he started the CONES Project—the first C modeling-based very large scale integration (VLSI) synthesis tool at India's premier electronics company, Bharat Electronics Ltd., Bangalore, where he had developed several high-speed and high-voltage analog integrated circuits intended for consumer electronics products. He is the author or coauthor of more than 200 technical papers and four books on various aspects of VLSI research works. His current research interests include current problems in nanoscale CMOS VLSI design, computer-aided design (CAD) tools, and circuit designs for emerging technologies including quantum MOS and resonant tunneling devices, semiconductor memory systems, and physical synthesis of VLSI chips.

Dr. Mazumder is a Fellow of American Association for the Advancement of Science during 2008. He was a recipient of the Digital's Incentives for Excellence Award, BF Goodrich National Collegiate Invention Award, and Defense Advanced Research Projects Agency Research Excellence Award.